Elastic and inelastic α scattering on ^{36}Ar at $E_\alpha = 40$, 48, and 54 MeV

K. Kocher, R. Neu, F. Hoyler, H. Abele, P. Mohr, and G. Staudt
Physikalisches Institut der Universität Tübingen, D-7400 Tübingen, Germany

P. D. Eversheim and F. Hinterberger
Institut für Strahlen- und Kernphysik der Universität Bonn, D 5300 Bonn, Germany
(Received 15 July 1991)

Differential cross sections for elastic and inelastic α- scattering on ^{36}Ar have been measured at 40, 48, and 54 MeV. The data have been analyzed in the coupled-channel approach using double-folded optical α-^{36}Ar potentials considering the model of the symmetric rotator and the harmonic vibrator. The octupole transition probability deduced in the harmonic-vibrator model is almost identical to the value obtained from electromagnetic probes. In the symmetric-rotator model only the choice of negative β_2 and β_4 deformation parameters results in consistent fits to the data at all incident energies. This unambiguously proves the oblate shape of ^{36}Ar. The volume integrals and rms radii of the extracted optical potentials fit well into the systematics obtained for lighter *sd*-shell nuclei.

PACS number(s): 25.55.Ci, 24.10.Eq, 24.10.Ht

I. INTRODUCTION

A survey of the spectroscopic electric quadrupole moments for even-even nuclei in the *sd* shell [1] indicates that the nuclei ^{20,22}Ne, ^{24,26}Mg, ^{30}Si, and ^{32}S are prolate ($Q_{2^+} < 0$), whereas the ^{28}Si nucleus has a strong oblate deformation. The Q_{2^+} values for ^{34}S and ^{40}Ar are small, thus indicating a nearly spherical shape. The static quadrupole moment of the first excited state in ^{36}Ar has been measured by the reorientation effect in Coulomb excitation [2]. The experimental result ($Q_{2^+} = 11 \pm 6$ e fm^2) indicates an oblate shape for ^{36}Ar.

The analysis of $(\vec{d},d')$ data on ^{36}Ar using coupled-channel (CC) calculations [3] in the symmetric-rotational model shows practically no difference between the two signs of the deformation parameter β_2. Furthermore, there are no significant differences between the rotational and the vibrational calculations.

The excitation of collective states in inelastic α scattering allows one to extract information on nuclear deformation and on transition probabilities. In a recent CC analysis of inelastic scattering of 54-MeV α particles on ^{19}F, ^{20,22}Ne, ^{23}Na [4], and ^{24}Mg [5], we have extracted B(IS2), B(IS4), and Q_{2^+} values which compare favorably with experimental values obtained from electromagnetic probes and shell-model calculations.

In the present investigation we measured the elastic and inelastic α scattering on ^{36}Ar at incident energies of about 40, 48, and 54 MeV. First, the elastic data together with existing data at lower incident energy of Gaul *et al.* [6] are analyzed in the framework of the conventional optical model. Second, the results of the present experiment are analyzed within the CC method using the quadrupole, octupole, and hexadecapole transition amplitudes evaluated from the harmonic-vibrational model (HVM) as well as using quadrupole and hexadecapole transition amplitudes evaluated from the symmetric-rotational model (SRM). The main emphasis of this investigation is the extraction of B(ISλ) values and quadrupole moments and the comparison of these results with other measurements and calculations.

All calculations have been performed using double-folded optical α-^{36}Ar potentials. Our previous, above-mentioned, investigations [4,5] result in a very systematic behavior of the α- nucleus optical potentials for nuclei in the mass range between $A = 13$ and $A = 24$. The second aim of this paper is thus the determination of the α-nucleus potential for ^{36}Ar.

II. EXPERIMENT

The measurements were performed at the isochronous cyclotron of the University of Bonn. The incident energies of the α-particle beam were 40.0, 48.3, and 53.7 MeV. Beam intensities between 30 and 870 nA were used with an energy resolution of 5×10^{-4}. A cylindrical gas cell of 60-mm diameter containing the isotopically enriched (99.8%) ^{36}Ar target gas was centered in the 50-cm-diameter scattering chamber. The gas pressure was monitored continuously. The detector system consisted of four E detectors mounted on two turntables rotating around the target. The detectors were of the surface-barrier type with a thickness of 1500–2000 μm. The dead time was monitored continuously with a random pulser. The spectra were accumulated in a computer and stored on magnetic tapes for further off-line processing. The energy resolution in the particle spectra was about 250–300 keV. A peak-fitting technique was applied to separate the excited state at 4.18 MeV (3_1^-) from the multiplet of states [7] at 4.33 [(0_2^+)], 4.41 (4_1^+), and 4.44 MeV (2_2^+). (See Fig. 1.) The evaluation of the measurements followed closely the procedure outlined by Silverstein [8]. Data were accumulated at 40 MeV for laboratory angles from 11° to 170° in 1° steps, at 48 MeV for 15° to 40° in 0.5° steps and 40° to 160° in 1° steps, and finally

at 54 MeV for 10° to 50° in 0.5° steps and 50° to 162° in 1° steps. The zero-degree direction could be determined with an accuracy of $\pm 0.2°$ by using the method described in Ref. [9]. Beam monitoring was accomplished in the usual way by means of a Faraday cup. The comparison with the 41-MeV scattering data of Boschitz *et al.* [10] shows good agreement with our 40-MeV data in the absolute normalization.

III. OPTICAL-MODEL ANALYSIS

First we consider the description of the elastic α scattering in the optical model (OM). The obtained elastic differential cross sections are shown in Fig. 2 together with the data of Gaul *et al.* [6] at energies between 18 and 29 MeV.

The real part of the optical potential was deduced in the framework of the double-folding model of Kobos *et al.* [11] and is described by

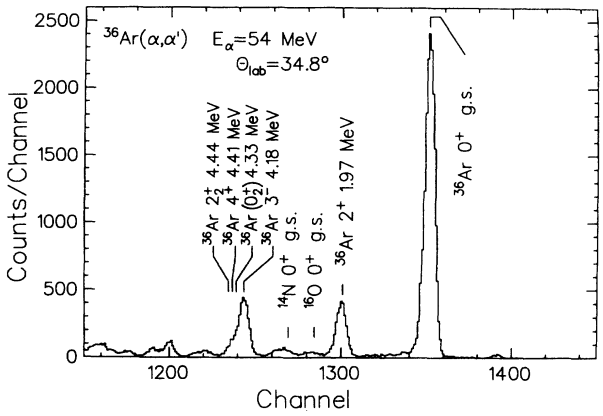

FIG. 1. Typical ^{36}Ar-α spectrum at 34.8° and $E_\alpha = 54$ MeV.

$$V(r) := U_F(r) = \lambda_f \int d\mathbf{r}_1 \int d\mathbf{r}_2 \rho_T(\mathbf{r}_1)\rho_\alpha(\mathbf{r}_2) t(E,\rho_T,\rho_\alpha,\mathbf{s}=\mathbf{r}+\mathbf{r}_2-\mathbf{r}_1) , \quad (1)$$

where $\mathbf{r}$ is the separation of the centers of mass of the colliding target nucleus and the α particle, $\rho_T(\mathbf{r}_1)$ and $\rho_\alpha(\mathbf{r}_2)$ are the respective nucleon densities, $t(E,s)$ is the density-dependent effective interaction, and λ_f is an overall normalization factor. For the density distribution of the target nucleus ρ_T we used the experimental charge distribution [12] obtained from electron scattering and unfolded from the finite charge distribution of the proton. Since $N=Z$ for ^{36}Ar, neutron and proton distributions can be assumed to be identical. For the density distribution of the α particle a Gaussian form was used [13]. A detailed description of the computation of the potential $U_F(r)$ is given in Ref. [9]. The radial dependence of the imaginary potential was taken as a sum of a Woods-Saxon volume and surface term. This parametrization turned out to be more successful than the use of a Fourier-Bessel series with the same number of adjustable parameters.

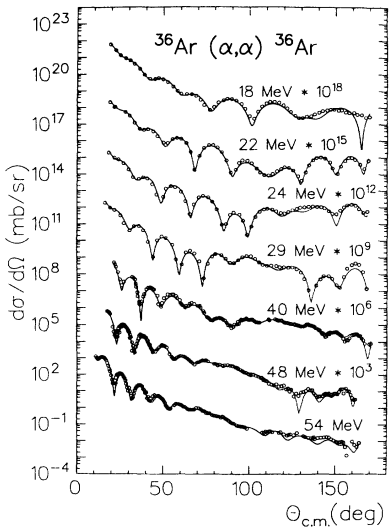

FIG. 2. Elastic α scattering on ^{36}Ar. Experimental data and optical-model fits were calculated by using the double-folding potentials at incident energies of 18.0, 22.1, 24.1, 29.2 [6] and 40.0, 48.3, 53.7 MeV (this work).

All fits were performed using the computer code GOMFIL [14], where in our case only the normalization factor λ_f of the real part and the six Woods-Saxon parameters of the imaginary part of the potential are adjustable parameters. The results of the OM calculations are shown in Fig. 2. For the whole energy range a good agreement between experimental and calculated data has been found.

The normalization factor λ_f and the potential parameters obtained in this analysis are listed in Table I. For the imaginary potentials one observes an increase in the surface absorption with increasing energy. At 54 MeV the shape of the imaginary potential is almost given by the surface Woods-Saxon term. Calculations with potentials similar to that at 48 MeV lead to a deterioration in the description of the experimental data. Nevertheless, the values for the different potentials are very similar for radii larger than 5 fm. The normalization factor λ_f, and as a consequence the volume integral $J_R/4A$ of the real part of the potential, decrease with increasing energy, whereas the volume integrals and the rms radii of the imaginary potential show a marked increase with increasing energy. Even at 54 MeV, where the shape of the imaginary potential is different, the systematic behavior persists. The rms radii of the real part are, due to the folding procedure, constant within 0.1% over the whole energy range. The volume integrals per nucleon and the rms radii for both

TABLE I. Normalization factor λ_f of the real part and potential parameters of the imaginary part of the optical potential.

E_{lab} (MeV)	λ_f	W_V (MeV)	r_V (fm)	a_V (fm)	W_D (MeV)	r_D (fm)	a_D (fm)
18	1.303	12.49	1.505	0.138	0.36	2.274	0.613
22	1.300	11.09	1.528	0.152	0.64	2.228	0.582
24	1.293	11.55	1.543	0.126	0.69	2.229	0.455
29	1.323	12.55	1.492	0.156	1.63	1.856	0.761
40	1.321	22.94	1.169	1.025	6.25	1.396	0.260
48	1.320	32.86	0.903	1.233	13.74	1.324	0.300
54	1.270	2.12	2.249	0.753	49.29	1.225	0.342

the real and the imaginary part of the optical potential are listed in Table II.

IV. COUPLED-CHANNEL ANALYSIS

In order to obtain further insight into the nature of the low-lying collective states of the ^{36}Ar nucleus, we have applied the coupled-channel formalism developed by Tamura [15] to the inelastic scattering data. Following Tamura the coupling matrix elements can be expressed in the general form

$$\langle l_f I_f | V_{cp} | l_i I_i \rangle = \sum_{\lambda \neq 0} v_\lambda^{cp}(r) \langle I_f \| Q_\lambda \| I_i \rangle \times A(l_f I_f, l_i I_i, \lambda I) . \quad (2)$$

The factors $A(l_f I_f, l_i I_i, \lambda I)$ are purely geometric and model independent. In contrast, the other two factors, namely, the radial form factor $v_\lambda^{cp}(r)$ and the reduced matrix elements $\langle I_f \| Q_\lambda \| I_i \rangle$, are model dependent.

A. First-order harmonic-vibrational model

The vibrational model describes the dynamical deformation of the spherical surface of the nucleus by the parametrization

$$R(\vartheta,\varphi) = R_0 \left[1 + \sum_{\lambda\mu} \alpha_{\lambda\mu} Y_{\lambda\mu}(\vartheta,\varphi) \right] . \quad (3)$$

By expanding the potential in powers of $Y_{\lambda\mu}(\vartheta,\varphi)$ to first order we obtain

$$V(r-R) = V(r-R_0) + \sum_{\lambda\mu} R_0 \frac{\partial V}{\partial r}(r-R_0) \alpha_{\lambda\mu} Y_{\lambda\mu}(\vartheta,\varphi) = V_{diag} + V_{cp} . \quad (4)$$

TABLE II. Volume integrals and rms radii for the optical-model analysis.

E_{lab} (MeV)	J_R (MeV fm^3)	$\langle r_R^2 \rangle^{1/2}$ (fm)	J_I (MeV fm^3)	$\langle r_I^2 \rangle^{1/2}$ (fm)
18	366.9	4.11	49.3	4.37
22	363.9	4.11	48.8	4.66
24	360.9	4.11	50.6	4.55
29	366.3	4.11	60.8	4.84
40	360.1	4.11	76.7	4.73
48	355.1	4.11	95.5	4.78
54	338.7	4.11	125.7	4.78

Generally, the coupling potential V_{cp} can be expressed as

$$V_{cp} = \sum_{\lambda\mu} v_\lambda^{cp}(r) Q_{\lambda\mu} Y_{\lambda\mu}(\vartheta,\varphi) . \quad (5)$$

Thus, the radial form factor is given as $v_\lambda^{cp}(r) = R_0(\partial V/\partial r)(r-R_0)$ and the transition operator as $Q_{\lambda\mu} = \alpha_{\lambda\mu}$. These dynamical deformation parameters $\alpha_{\lambda\mu}$ can be decomposed in the usual way into operators $b_{\lambda\mu}$ and $b_{\lambda\mu}^*$ which annihilate and create a phonon of vibration:

$$\alpha_{\lambda\mu} = \frac{\beta_\lambda}{\sqrt{2\lambda+1}} [b_{\lambda\mu} + (-)^\mu b_{\lambda-\mu}^*] . \quad (6)$$

Using these $b_{\lambda\mu}^*$ and denoting the ground state by $|0\rangle$, a one-phonon state with spin I and its projection M can be written as

$$|1;IM\rangle = b_{IM}^* |0\rangle . \quad (7)$$

The root-mean-square deformation parameter β_λ is defined in such a way that β_λ^2 stands for the expectation value of $\sum_\mu |\alpha_{\lambda\mu}|^2$ in the nuclear ground state:

$$\beta_\lambda^2 = \left\langle 0 \left| \sum_\mu |\alpha_{\lambda\mu}|^2 \right| 0 \right\rangle . \quad (8)$$

Using these dynamical deformation operators for the wave functions, the results for those reduced matrix elements which were used in this work are summarized as follows. For the transition with the multipolarity λ from the ground state to a one-phonon state we get

$$\langle 1;I \| Q_\lambda \| 0;0 \rangle = \delta_{\lambda I} (-)^I \beta_\lambda . \quad (9)$$

In the case of the transition from a one-quadrupole-phonon state to a two-quadrupole-phonon state the reduced matrix elements are given by

$$\langle 2;I \| Q_2 \| 1;2 \rangle = \beta_2 \left[\frac{2(2I+1)}{5} \right]^{1/2} . \quad (10)$$

In order to simulate anharmonicities, a mixing between two-phonon amplitudes and one-phonon amplitudes can be assumed in the construction of the triplet ($I = 0^+, 2^+, 4^+$) states [16].

$$|I\rangle_{triplet} = \cos\varphi_I |1;I\rangle + \sin\varphi_I |2;I\rangle . \quad (11)$$

The mixing allows a direct transition from the ground state to each of the triplet states.

The normalized multipole moments for a normalized axial-symmetric mass distribution $\rho(r)$ are given in the body-fixed system as

$$q_{\lambda 0} := \int \rho(\mathbf{r}) r^{\lambda} Y_{\lambda 0}(\Omega') d\mathbf{r} \ . \tag{12}$$

According to the Satchler theorem [17–19] the normalized mass distribution can be replaced by the normalized potential, if the real part V_R of the effective scattering potential can be described by a folding ansatz with a density-independent effective NN interaction (implicit folding procedure). Because the DD$M3Y$ interaction [11] is density dependent, the obtained multipole moments have to be corrected accordingly. The required correction factors c_λ have been calculated by Srivastava and Rebel [20]. Thus we get

$$q_{\lambda 0} = \frac{1}{c_\lambda} \frac{\int v_\lambda^{\rm cp}(r) r^{\lambda+2} dr}{4\pi \int V(r) r^2 dr} \ , \tag{13}$$

with the radial form factor $v_\lambda^{\rm cp}(r) = R_0(\partial V/\partial r)(r - R_0)$. By partial integration, and after multiplying with the nuclear charge Ze and the reduced matrix element, we obtain for the isoscalar transition probability

$$B(\mathrm{IS}\lambda, I_i \to I_f) = \frac{1}{2I_i+1} \left[\frac{R_0 \langle I_f \| Q_\lambda \| I_i \rangle Ze(\lambda+2) \int V(r) r^{(\lambda+1)} dr}{4\pi c_\lambda \int V(r) r^2 dr} \right]^2 \tag{14}$$

using the radial moments $\int V(r) r^{(\lambda+1)} dr$ of the undeformed real potential.

B. Symmetric-rotator model

For permanently deformed nuclei, the rotator model is adequate to analyze the inelastic data. Assuming an axial-symmetric quadrupole and hexadecapole deformation, the radius parameter $R(\Omega')$ in the body-fixed system is angle dependent according to

$$R(\Omega') = R_0[1 + \beta_2 Y_{20}(\Omega') + \beta_4 Y_{40}(\Omega')] \ . \tag{15}$$

The coupling potentials $V_{\rm cp}$ are derived from the Legendre polynomial expansion of the deformed interaction potential $V(r, R(\Omega'))$ transformed from the body-fixed (Ω') into the space-fixed (Ω) system:

$$V_{\rm cp}(r, \Omega) = \sum_{\substack{\lambda,\mu \\ \lambda \neq 0}} v_\lambda^{\rm cp}(r) D^\lambda_{\mu 0}(\varepsilon_i) Y_{\lambda\mu}(\Omega) \ , \tag{16}$$

where $D^\lambda_{\mu 0}(\varepsilon_i)$ are the Wigner rotation matrices, ε_i are the Euler angles, and

$$v_\lambda^{\rm cp}(r) = \int V(r, R(\Omega')) Y_{\lambda 0}(\Omega') d\Omega' \tag{17}$$

is the radial form factor which describes the radial shape of the transition potential. Comparing Eq. (16) with (5), the transition operators $Q_{\lambda\mu}$ are just the Wigner rotation matrices. Considering the ground-state band ($K=0$) of the ^{36}Ar nucleus and using the wave functions of a symmetric rotator we obtain for the reduced matrix elements

$$\langle I_f \| D^\lambda_{;0} \| I_i \rangle = (2I_i+1)^{1/2} (I_i \lambda 00 | I_f 0) \ . \tag{18}$$

The evaluation of the isoscalar transition probability within the rotator model [4,5] is similar to that of the vibrational model. Assuming that neutron and proton deformations are the same, one gets

$$B(\mathrm{IS}\lambda, I_i \to I_f) = \frac{1}{(2I_i+1)} M^2_{\mathrm{IS}\lambda}(I_i \to I_f) \ , \tag{19}$$

with the reduced isoscalar matrix elements

$$M_{\mathrm{IS}\lambda}(I_i \to I_f) = i^\lambda Z e q_{\lambda 0} \langle I_f \| D^\lambda_{;0} \| I_i \rangle \ , \tag{20}$$

where $q_{\lambda 0}$ is calculated by inserting Eq. (17) into Eq. (13). Finally, the diagonal IS2 matrix elements are related to the spectroscopic quadrupole moments of the excited nuclei by

$$eQ_I = \left[\frac{16\pi}{5} \frac{I(2I-1)}{(I+1)(2I+1)(2I+3)} \right]^{1/2} M_{\mathrm{IS}2}(I \to I) \ . \tag{21}$$

C. Coupled-Channel Calculations

The spectrum of ^{36}Ar shows the energy spacing of a harmonic vibrator. However, the transition rates [21] for $(0_2^+) \to 2_1^+$ and $2_2^+ \to 2_1^+$ are far from the value which results from the assumption of pure two-phonon triplet states. Additionally there is a direct γ-ray transition from the 2_2^+- state to the ground state [21]. This behavior can only be expected if there is an anharmonicity. On the other hand, the ratio of the $B(E2)$ values from $2_1^+ \to 0_1^+$ to $4_1^+ \to 2_1^+$ is almost equal to the value one expects from the Alaga rules for a rotational nucleus. Therefore we analyzed the experimental data within the rotational as well as within the vibrational model. The coupling schemes are shown in Fig. 3 for both models.

The numerical calculations were performed using a modified version of the computer code ECIS [22]. In order to gain a properly permanent deformed potential the double-folding potential is expanded in a Fourier-Bessel series of 20 terms, in which the cutoff radius R_c is described by the expansion (15). In all calculations the Coulomb potential is deformed in the usual way [15].

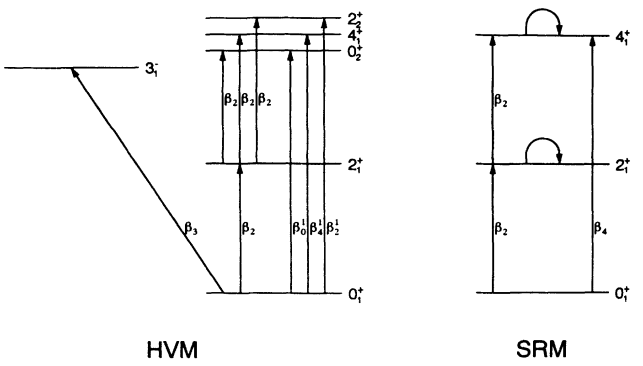

FIG. 3. Coupling scheme for the harmonic-vibrator model (HVM) and the symmetric-rotator model (SRM).

To obtain an optimum reproduction of the experimental cross-section data, first the deformation parameters β_λ and the potential parameters were adjusted for each energy. In a second step, the deformation parameters were fixed to an intermediate value for all energies.

In the vibrational model we assume a mixing of one- and two-phonon amplitudes for the triplet states. The mixing angles φ_0, φ_4, and φ_2 for the states (0_2^+), 4_1^+ and 2_1^+ have been deduced from the ratios of the electromagnetic transition rates from the triplet states to the first 2_1^+ state to the transition from the 2_1^+ state to the ground state:

$$\varphi_I = \arcsin\left[\frac{B(E2,I\rightarrow 2_1^+)}{2B(E2,2_1^+\rightarrow 0_1^+)}\right]^{1/2} . \quad (22)$$

With the experimental $B(E2)$ values [21,23] from Table VII one gets

$$\varphi_0 = 15.7^\circ, \quad \varphi_4 = 52.3^\circ, \quad \varphi_2 = 27.0^\circ .$$

These mixing angles have been kept constant throughout the analyses. Additionally β_0^1 has been set to 0 in order to reduce the number of free parameters in the fit. The values of $\beta_4^1 = 0.201$ and $\beta_2^1 = 0.081$ have only been fitted to the data at 40 MeV and kept fixed at these values for 48 and 54 MeV, because of the poorer data at these energies. For all transition potentials in the harmonic-vibrational model an equilibrium radius of $R_0 = 4.11$, equal to the rms radius of the undeformed folding potential, was used.

The final results for the calculations using the vibrational model are shown in Fig. 4. The theoretical differential cross sections of the triplet states are summed up for comparison with the experimental data.

The obtained potential parameters are shown in Table III; the deformation parameters used in the calculations are given in Table IV, together with the resulting volume integrals and rms radii of the potentials. The differential cross sections calculated with the averaged results for β_2 and β_3 shown in Fig. 4 are very similar to those obtained in the best-fit analyses carried out for each energy. The differences between the best-fit and averaged values of β_2 and β_3 are less than 5%; those in the volume integrals and the rms radii of the potentials are even slightly smaller.

In the analyses within the axial-symmetric-rotator model only the ground state and the 2_1^+ and 4_1^+ states are taken into account. We performed these calculations under the assumption that the main contribution to the experimentally unresolved triplet is from the 4_1^+ state. In the best-fit analyses carried out for each energy both signs for β_2 as well as for β_4 were allowed. Depending on the α energy, different combinations of the signs of β_2 and β_4 lead to acceptable fits, but only negative values for both β_2 and β_4 result in a good description of the experimental data in all cases. On the other hand, the combina-

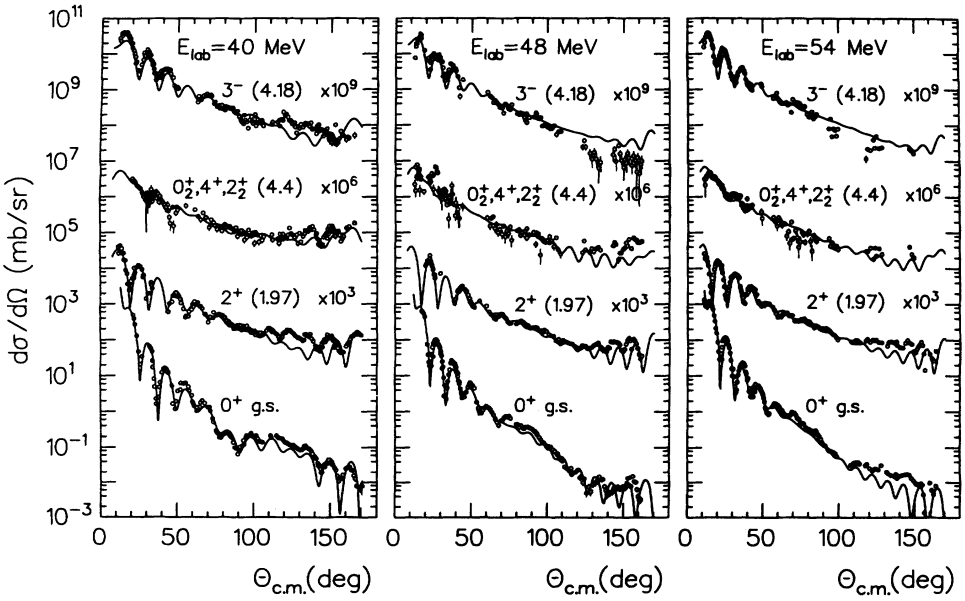

FIG. 4. Elastic and inelastic α scattering on ^{36}Ar at 40.0, 48.3, and 53.7 MeV. Experimental data and CC analysis fits were calculated with the double-folded potential within the first-order harmonic-vibrational model. For deformation parameters see Table IV.

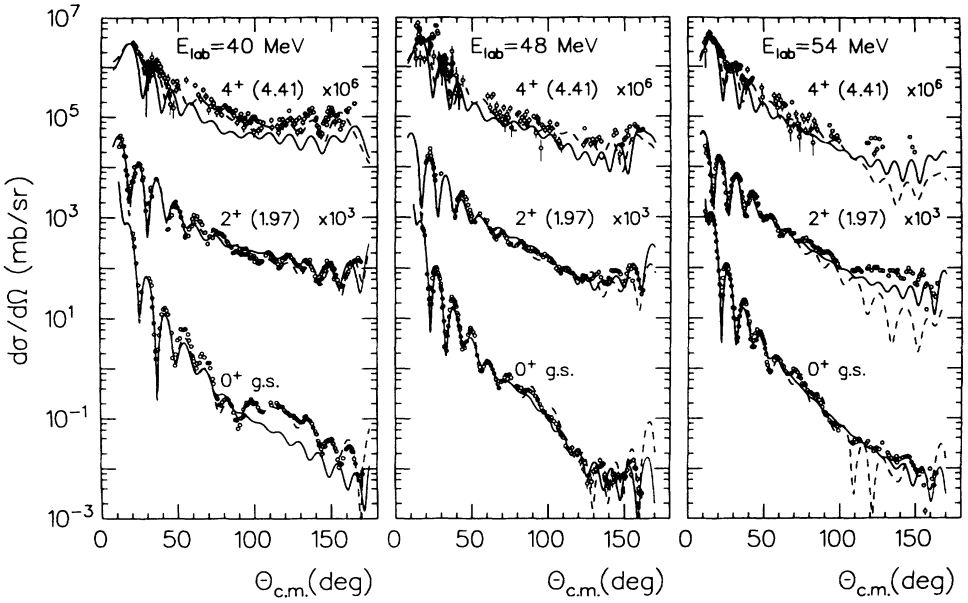

FIG. 5. Same as Fig. 4, but within the symmetric-rotator model. The deformation parameters are fixed at $\beta_2=-0.16$, $\beta_4=+0.07$ (solid line) and at $\beta_2=+0.16$, $\beta_4=-0.07$ (dashed line).

tion $\beta_2>0,\beta_4>0$ did not result in acceptable fits at all. To illustrate the effect of choosing different combinations of signs for the deformation parameters the cases $\beta_2=-0.16,\beta_4=+0.07$ (solid lines) and $\beta_2=+0.16$, $\beta_4=-0.07$ (dashed lines) are shown in Fig. 5. It can be seen that the combination $\beta_2<0,\beta_4>0$ gives a better description of the experimental data at 54 MeV, whereas at 40 MeV the choice $\beta_2>0,\beta_4<0$ provides a significantly better fit. At 48 MeV, both combinations do equally well.

In the best-fit analyses carried out with negative β_2 and β_4 parameters for each energy, very similar deformation parameters are observed. The final results, calculated with average absolute values for β_2 and β_4, are shown in Fig. 6. The potential parameters resulting from these analyses using averaged deformation parameters with negative sign are shown in Table V. The corresponding volume integrals and rms radii of the optical potentials are shown in Table VI together with the values for β_2 and β_4. As in the calculations using the vibrational model, here again the differences to the integral values obtained in the best-fit analyses are smaller than 5%.

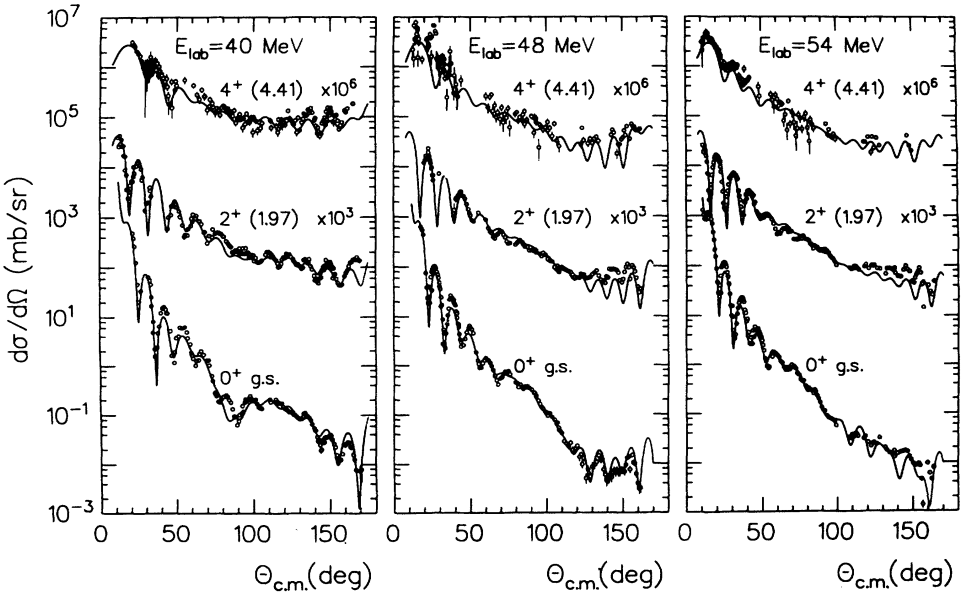

FIG. 6. Same as Fig. 5. The deformation parameters are fixed at $\beta_2=-0.208$, $\beta_4=-0.084$.

TABLE III. Normalization factor λ_f of the real part and parameters of the imaginary part of the potential within the vibrational model.

E_{lab} (MeV)	λ_f	W_V (MeV)	r_V (fm)	a_V (fm)	W_D (MeV)	r_D (fm)	a_D (fm)
40	1.467	19.37	1.331	0.598	0.562	1.839	0.562
48	1.520	10.39	1.343	1.013	29.93	0.792	0.402
54	1.500	2.10	1.928	0.902	30.35	0.822	0.705

TABLE IV. Deformation parameters, volume integrals, and rms radii within the vibrational model. The mixing angles are $\varphi_0=15.7°$, $\varphi_4=52.3°$, and $\varphi_2=27.0°$. The deformation parameters for the one-phonon component of the triplet states are $\beta_0^1=0.0$, $\beta_4^1=0.201$, and $\beta_2^1=0.081$. For the transition potentials $R_0=4.11$ was chosen.

E_{lab} (MeV)	β_2 (fm)	β_3 (fm)	J_R (MeV fm^3)	$\langle r_R^2\rangle^{1/2}$ (fm)	J_I (MeV fm^3)	$\langle r_I^2\rangle^{1/2}$ (fm)
40	0.239	0.247	400.3	4.11	59.0	4.18
48	0.239	0.247	409.2	4.11	70.5	4.25
54	0.239	0.247	400.4	4.11	85.6	4.40

TABLE V. Normalization factor λ_f of the real part and parameters of the imaginary part of the potential within the rotational model.

E_{lab} (MeV)	λ_f	W_V (MeV)	r_V (fm)	a_V (fm)	W_D (MeV)	r_D (fm)	a_D (fm)
40	1.306	19.52	1.162	1.003	1.74	1.211	0.382
48	1.278	26.22	1.077	1.085	12.06	1.053	0.208
54	1.249	9.04	1.616	1.010	42.50	1.014	0.217

TABLE VI. Deformation parameters, volume integrals, and rms radii within the rotational model.

E_{lab} (MeV)	β_2	β_4	J_R (MeV fm^3)	$\langle r_R^2\rangle^{1/2}$ (fm)	J_I (MeV fm^3)	$\langle r_I^2\rangle^{1/2}$ (fm)
40	−0.208	−0.084	356.3	4.11	57.1	4.65
48	−0.208	−0.084	344.0	4.11	76.0	4.60
54	−0.208	−0.084	333.4	4.11	89.8	4.72

TABLE VII. $B(\mathrm{IS}\lambda)$ and $B(E\lambda)$ values in units of $e^2\mathrm{fm}^{2\lambda}$ and the static quadrupole moment Q_2.

			$B(\mathrm{IS}\lambda)$		$B(E\lambda)$	
I_i	I_f	λ	Vibrator	Rotator	Shell model[a]	Expt.[b]
2_1^+	0_1^+	2	80	80	49	68±8[c]
(0_2^+)	2_1^+	2	12	· · ·		10±9
2_2^+	2_1^+	2	33	· · ·	19	28±13
4_1^+	2_1^+	2	99	114		85±14
2_2^+	0_1^+	2	7	· · ·		2.8±0.5
3_1^-	0_1^+	3	1600	· · ·		1600±200[d]
4_1^+	0_1^+	4	9300	3500	6900[e]	
2_1^+ Q_2 (e fm^2)		· · ·	+18	+12	+11±6[f]	

[a]Reference [27].
[b]Reference [21].
[c]Reference [23].
[d]Reference [24].
[e]Reference [25].
[f]Reference [2].

V. DISCUSSION

Comparing the CC analyses, using the HVM and the SRM, we can find as a first result that the quality of the fits to the ground state is good in both models. For c.m. angles greater than 100° the description within the SRM is more successful because analyses within the HVM underestimate the data (54 MeV) or are out of phase (48 MeV).

For the first 2^+ state, which could be analyzed in both models, the SRM, using negative values for β_2 and β_4, describes the oscillatory pattern of the large-angle data much better than the HVM.

The description of the 4^+ state within the SRM is also very satisfactory for all three energies and the whole angular range. The relatively broad oscillation in forward direction is especially nicely reproduced. The comparison of Fig. 5 and Fig. 6 shows again that negative deformation parameters are clearly favored. With the negative sign of β_2 one obtains a spectroscopic quadrupole moment of the first excited state of $+18$ e fm^2, which is in agreement with the result at $+11(6)$ e fm^2 obtained in Coulomb excitation [2] and establishes the oblate deformation of ^{36}Ar.

The 0_2^+-4_1^+-2_2^+ triplet is also described very well for all three energies in the HVM, although, as stated in Sec. IV C, the deformation parameters β_4^1 and β_2^1 were fitted only at 40 MeV. The description of the 3^- state is also reasonable, whereas for larger angles the cross section seems to be overestimated.

The comparison of the $B(\mathrm{IS}\lambda)$ values with the experimental $B(E\lambda)$ values in Table VII shows a good agreement between the $B(\mathrm{IS3})$ and the $B(E3)$ value [24], whereas the $B(E2)$ values [21,23] are slightly overestimated by both models in spite of having been corrected for effects from the density dependence of the effective NN interaction. Nevertheless, the $B(\mathrm{IS2})$ values and also the quadrupole moment are only somewhat larger than the upper boundary for the electromagnetic values [2,21,23]. For the $E4$ transition $0^+ \rightarrow 4^+$ there are no experimental values from the literature, but Brown *et al.* [25] derived from shell-model calculations a value of $M_4(0 \rightarrow 4) = -248$ e fm^4, which is in reasonable agreement with the value of $M_{\mathrm{IS4}}(0 \rightarrow 4) = -176$ e fm^4 extracted from our experimental data within the SRM.

In both models the shapes of the obtained imaginary potentials (Tables III and V) show nearly the same feature as the potentials obtained in the OM analysis of Sec. III. The corresponding volume integrals (Table IV and VI) are identical within a few percent and increase with increasing energy. Compared to the volume integrals from the optical-model calculations (Table II) they are lower by 20–30 %, due to the explicit consideration of the first excited states. The values are similar to those obtained from α scattering on nuclei at the beginning of the *sd* shell [4].

For the real part of the optical potential the two models gave a different behavior: in the vibrational model the volume integrals are higher than those from the optical-model calculations, while they are lower for calculations in the rotational model.

This decrease of the real potential for nuclei with an oblate shape in CC calculations compared to pure optical-model calculations has already been observed by Clement *et al.* [26].

Comparing the analyses within the two models, the SRM seems to be better suited for the description of inelastic α scattering. First, the overall description of the differential cross sections is better in the SRM. Also the $B(\mathrm{IS2})$ values are almost correct without any artificial assumption. Second, the calculations in the HVM treating the triplet as pure two-phonon states (not displayed in this work) underestimates the experimental cross section of the multiplet by a factor of about 2, although the extracted $B(\mathrm{IS2})$ values are much too high compared with the electromagnetic values. Only the introduction of one-phonon amplitudes to the triplet leads to satisfactory results. Third, the value of the renormalization factor λ_f of the folding potential seems to be too high in the HVM calculations, compared to the systematics deduced for lighter nuclei [4].

VI. CONCLUSIONS

Differential cross sections for the elastic and inelastic scattering of α particles on ^{36}Ar have been measured at the incident energies of 40.0, 48.3, and 53.7 MeV. The elastic-scattering data have been analyzed in the framework of the optical model together with data at lower energies [6] using a double-folded real potential. The angular distributions are described very satisfactorily for all incident energies between 18 and 54 MeV. The integral values of the optical potentials show a smooth variation with energy.

The inelastic scattering was treated in the vibrational as well as in the rotational model. Again the real optical potential was deduced from the folding procedure.

While the inelastic scattering to the 3^- state is described reasonably well in the vibrational model, the description of the scattering to the 2_1^+ and the 4_1^+ state is better in the rotational model. Here negative values for β_2 and for β_4 are needed to fit the inelastic scattering data at all three energies. The spectroscopic quadrupole moment of the 2_1^+ state is found to be positive, thus showing the oblate shape of ^{36}Ar. The extracted isoscalar quadrupole transition strength to the first excited 2^+ state has the same value for both models but is slightly higher than the electromagnetic value. Through the mixing of one- and two-phonon amplitudes for the triplet states the ratio of the two amplitudes is fixed, but their absolute values and the strength of the one-phonon transition can be extracted. For the transition $0^+ \rightarrow 3^-$ the $B(\mathrm{IS3})$ value extracted from the vibrational model is in excellent agreement with the $B(E3)$ value from inelastic electron scattering. In the case of the hexadecapole transition from the ground state to the first 4^+ state the negative theoretical value for the reduced matrix element confirms the negative β_4 value from our analyses. The theoretical value from the shell model lies in between our results for the HVM and the SRM. Because of the overall better description of the differential cross sections and the more consistent behavior of the extracted transition rates as

well as the optical potentials, the SRM seems to be better suited for the description of inelastic α scattering.

In this investigation it has been shown that the use of a double-folded optical α-nucleus potential in the coupled-channel approach is a sensitive tool for obtaining information on nuclear deformation and isoscalar transition probabilities, provided an extensive set of experimental data is available. The systematic behavior of the parameters entering the calculations make the transition probabilities very reliable.

ACKNOWLEDGMENTS

The cooperation of the Bonn Isochronous Cyclotron team is gratefully acknowledged. This work has been funded by the German Federal Minister for Research and Technology at Bundesministerium für Forschung und Technologie (BMFT) under Contract No. 06 Tü 460.

[1] P. Rhagavan, At. Data Nucl. Data Tables **42**, 189 (1989).
[2] K. Nakai, F. S. Stephens, and R. M. Diamond, Phys. Lett. **34B**, 389 (1971).
[3] J. Nurzynski, T. Kihm, K. T. Knöpfle, G. Mairle, and H. Clement, Nucl. Phys. **A465**, 365 (1987).
[4] J. Fritze, R. Neu, H. Abele, F. Hoyler, G. Staudt, P. D. Eversheim, F. Hinterberger, and H. Müther, Phys. Rev. C **43**, 2307 (1991).
[5] R. Neu, S. Welte, H. Clement, H. J. Hauser, G. Staudt, and H. Müther, Phys. Rev. C **39**, 2145 (1989).
[6] G. Gaul, H. Lüdecke, R. Santo, H. Schmeing, and R. Stock, Nucl. Phys. **A137**, 177 (1969).
[7] P. M. Endt and C. van der Leun, Nucl. Phys. **A310**, 1 (1978).
[8] E. Silverstein, Nucl. Instrum. Methods **4**, 53 (1959).
[9] H. Abele, H. J. Hauser, A. Körber, W. Leitner, R. Neu, H. Plappert, T. Rohwer, G. Staudt, M. Strasser, S. Welte, M. Walz, P. D. Eversheim, and F. Hinterberger, Z. Phys. A **326**, 373 (1987).
[10] E. T. Boschitz, J. S. Vincent, R. W. Bercaw, and J. R. Priest, Phys. Rev. Lett. **13**, 442 (1964).
[11] A. M. Kobos, B. A. Brown, R. Lindsay, and R. Satchler, Nucl. Phys. **A425**, 205 (1984).
[12] H. de Vries, C. W. de Jager, C. de Vries, At. Data Nucl. Data Tables **36**, 495 (1987).
[13] G. R. Satchler and W. G. Love, Phys. Rep. **55**, 183 (1979).
[14] H. Leeb, computer code GOMFIL, Technical University of Vienna (unpublished).
[15] T. Tamura, Rev. Mod. Phys. **37**, 679 (1965).
[16] T. Tamura, Prog. Theor. Phys. Suppl. **37/38**, 383 (1966).
[17] G. R. Satchler, J. Math. Phys. **13**, 1118 (1972).
[18] R. S. Mackintosh, Nucl. Phys. **A266**, 379 (1976).
[19] H. Rebel, Z. Phys. A **277**, 35 (1976).
[20] D. K. Srivastava and H. Rebel, Z. Phys. A **316**, 225 (1984).
[21] P. M. Endt, At. Data Nucl. Data Tables **23**, 3 (1979).
[22] J. Raynal, computer code ECIS, CEN Saclay (unpublished).
[23] S. Raman, C. W. Nestor, Jr., S. Kohane, and K. H. Bhatt, At. Data Nucl. Data Tables **42**, 1 (1989).
[24] R. H. Spear, At. Data Nucl. Data Tables **42**, 55 (1989).
[25] B. A. Brown, W. Chung, and B. H. Wildenthal, Phys. Rev. C **21**, 2600 (1980).
[26] H. Clement, G. Graw, W. Kretschmer, and W. Stach, J. Phys. Jpn. Suppl. **44**, 570 (1977).
[27] M. Carchidi, B. H. Wildenthal, and B. A. Brown, Phys. Rev. C **34**, 2280 (1986).